Draft version October 28, 2022
Typeset using LaTeX **twocolumn** style in AASTeX631

Constrain the Merger History of Primordial-Black-Hole Binaries from GWTC-3

Lang Liu,[1,2] Zhi-Qiang You,[1,2] You Wu,[3] and Zu-Cheng Chen[1,2]

[1] *Department of Astronomy, Beijing Normal University, Beijing 100875, China*
[2] *Advanced Institute of Natural Sciences, Beijing Normal University, Zhuhai 519087, China*
[3] *College of Mathematics and Physics, Hunan University of Arts and Science, Changde, 415000, China*

ABSTRACT

Primordial black holes (PBHs) can be not only cold dark matter candidates but also progenitors of binary black holes (BBHs) observed by LIGO-Virgo-KAGRA (LVK) Collaboration. The PBH mass can be shifted to the heavy distribution if multi-merger processes occur. In this work, we constrain the merger history of PBH binaries using the gravitational wave (GW) events from the third GW Transient Catalog (GWTC-3). Considering four commonly used PBH mass functions, namely the log-normal, power-law, broken power-law, and critical collapse forms, we find that the multi-merger processes make a subdominant contribution to the total merger rate. Therefore, the effect of merger history can be safely ignored when estimating the merger rate of PBH binaries. We also find that GWTC-3 is best fitted by the log-normal form among the four PBH mass functions and confirm that the stellar-mass PBHs cannot dominate cold dark matter.

1. INTRODUCTION

The successful detection of gravitational waves (GWs) from compact binary coalescences (Abbott et al. 2019, 2021a,b) has led us into a new era of GW astronomy. According to the recently released third GW Transient Catalog (GWTC-3) (Abbott et al. 2021b) by LIGO-Virgo-KAGRA (LVK) Collaboration, there are 90 GW events detected during the first three observing runs. Most of these events are categorized as binary black hole (BBH) mergers, and the BBHs detected by LVK have a broad mass distribution. The heaviest event, GW190521 (Abbott et al. 2020), has component masses $m_1 = 85^{+21}_{-14} M_\odot$ and $m_2 = 66^{+17}_{-18} M_\odot$. Both masses lie within upper black hole mass gap originated from pulsation pair-instability supernovae (Marchant et al. 2019), and current modelling places the lower cutoff of the mass gap at $\sim 50 \pm 4 M_\odot$ (Marchant et al. 2019; Farmer et al. 2019, 2020; Marchant & Moriya 2020). Even accounting for the uncertainties in modelling, it still implies at least m_1 is well within the mass gap and cannot have originated directly from a stellar progenitor (Anagnostou et al. 2020). Therefore, the heavy event GW190521 greatly challenges the stellar evolution scenario of astrophysical black holes.

Besides the astrophysical black holes, another possible explanation for the LVK BBHs is the primordial black holes (PBHs) (Bird et al. 2016; Sasaki et al. 2016; Chen & Huang 2018; Chen et al. 2022b). PBHs are black holes formed in the very early Universe through the gravitational collapse of the primordial density fluctuations (Hawking 1971; Carr & Hawking 1974). The formation of PBHs would inevitably accompany the production of scalar-induced GWs (Yuan et al. 2019, 2020a,b; Chen et al. 2020; De Luca et al. 2019; Bartolo et al. 2019b,a). PBHs can also be natural candidates of cold dark matter. Recent studies (Chen et al. 2022b,a) show that the BBHs from GWTC-3 are consistent with the PBH scenario, and the abundance of PBH in CDM, $f_{\rm pbh}$, should be in the order of $\mathcal{O}(10^{-3})$ to explain LVK BBHs. In particular, the merger rate for GW190521 derived from the PBH model is consistent with that inferred by LVK, indicating that GW190521 can be a PBH binary (Chen et al. 2022b).

liulang@bnu.edu.cn

zhiqiang.you@bnu.edu.cn

youwuphy@gmail.com

Corresponding author: zucheng.chen@bnu.edu.cn

Accurately estimating the merger rate distribution of PBH binaries can be crucial to extract the PBH population parameters from GW data. Liu et al. (2019) study the multi-merger processes of PBH binaries and show that the merger history of PBH binaries may shift the mass distribution from light mass to heavy mass depending on the values of population parameters. Wu (2020) then infers the population parameters of PBH binaries by accounting for the merger history effect using 10 BBHs from GWTC-1, finding that the effect of merger history can be safely ignored when estimating the merger rate of PBH binaries. In this work, we use the LVK recent released GWTC-3 data to constrain the effect of merger history on the merger rate of PBH binaries assuming all LVK BBHs are of primordial origin. We extend the analyses of Wu (2020) in several aspects. Firstly, we use GWTC-3, which expands GWTC-1 with almost six times more BBH events. The GWTC-3 events expand the mass and redshift coverage and can alleviate the statistical bias by including significantly more BBHs. Secondly, Wu (2020) only consider the PBH mass functions with the log-normal and power-law forms. We do more comprehensive analyses by including the broken power-law and critical collapse PBH mass functions that were not considered in Wu (2020). It is claimed by Deng (2021) that a broken power-law can fit the GW data better than the log-normal form. Lastly, we consider the redshift distribution of the merger rate that was ignored in Wu (2020).

We organize the rest paper as follows. In Sec. 2, we briefly review the calculation of the merger rate of PBH binaries by accounting for the merger history effect. In Sec. 3, we describe the hierarchical Bayesian framework used to infer the PBH population parameters from GW data. In Sec. 4, we consider four commonly used PBH mass functions and present the results. Finally, we give conclusions in Sec. 5.

2. MERGER RATE DENSITY DISTRIBUTION OF PBH BINARIES

In this section, we will outline the calculation of merger rate density when considering the PBH merger history effect. We refer to Liu et al. (2019) for more details.

The BBHs observed by LVK suggest that BHs should have a broad mass distribution, so we consider an extended mass function for PBHs. Here, we demand the probability distribution function of PBH mass, $P(m)$, be normalized such that

$$\int_0^\infty P(m)\,\mathrm{d}m = 1. \tag{1}$$

Assuming the fraction of PBHs in CDM is $f_{\rm pbh}$, we can estimate the abundance of PBHs in the mass interval $(m, m+\mathrm{d}m)$ as (Chen et al. 2019)

$$0.85 f_{\rm pbh}\, P(m)\,\mathrm{d}m. \tag{2}$$

The coefficient 0.85 is roughly the fraction of CDM in the non-relativistic matter, including both CDM and baryons. Following Liu et al. (2019), we may define an average PBH mass, $m_{\rm pbh}$, as

$$\frac{1}{m_{\rm pbh}} = \int \frac{P(m)}{m}\mathrm{d}m. \tag{3}$$

Then, we can obtain the average number density of PBHs with mass m in the total number density of PBHs, $F(m)$, by (Liu et al. 2019)

$$F(m) = P(m)\frac{m_{\rm pbh}}{m}. \tag{4}$$

We can now estimate the merger rate densities of PBH binaries by considering the merger history effect. We assume that PBHs are randomly distributed in the early Universe when they decouple from the cosmic background evolution (Nakamura et al. 1997; Sasaki et al. 2016; Ali-Haïmoud et al. 2017). The two nearest PBHs would attract each other because of the gravitational interactions. These two PBHs would obtain the angular momentum from the torque of other PBHs and form a PBH binary. The binary would emit gravitational radiations and eventually merge.

We do not intend to give a detailed derivation but quote the results from Liu et al. (2019) here. The merger rate density from first-merger process, $\mathcal{R}_1(t, m_i, m_j)$, is given by (Liu et al. 2019)

$$\mathcal{R}_1(t, m_i, m_j) = \int \hat{\mathcal{R}}_1 \mathrm{d}m_l, \tag{5}$$

where

$$\hat{\mathcal{R}}_1(t, m_i, m_j, m_l) \equiv 1.32\times10^6 \times \left(\frac{t}{t_0}\right)^{-\frac{34}{37}} \left(\frac{f_{\rm pbh}}{m_{\rm pbh}}\right)^{\frac{53}{37}} \times m_l^{-\frac{21}{37}} (m_i m_j)^{\frac{3}{37}} (m_i+m_j)^{\frac{36}{37}} F(m_i)F(m_j)F(m_l). \tag{6}$$

Similarly, the merger rate density from second-merger process, $\mathcal{R}_2(t, m_i, m_j)$, is given by (Liu et al. 2019)

$$\mathcal{R}_2(t, m_i, m_j) = \frac{1}{2}\int \hat{\mathcal{R}}_2(t, m_i - m_e, m_e, m_j, m_l)\ \mathrm{d}m_l \mathrm{d}m_e + \frac{1}{2}\int \hat{\mathcal{R}}_2(t, m_j - m_e, m_e, m_i, m_l)\ \mathrm{d}m_l \mathrm{d}m_e, \tag{7}$$

where

$$\hat{\mathcal{R}}_2(t, m_i, m_j, m_k, m_l) = 1.59 \times 10^4 \times \left(\frac{t}{t_0}\right)^{-\frac{31}{37}} \left(\frac{f_{\rm pbh}}{m_{\rm pbh}}\right)^{\frac{69}{37}} \times m_k^{\frac{6}{37}} m_l^{-\frac{42}{37}} (m_i + m_j)^{\frac{6}{37}} (m_i + m_j + m_k)^{\frac{72}{37}} \times F(m_i)F(m_j)F(m_k)F(m_l). \tag{8}$$

We only consider the effect of merger history up to the second-merger process. Therefore the total merger rate density, $\mathcal{R}(t, m_i, m_j)$, of PBH binaries at cosmic time t with masses m_i and m_j is

$$\mathcal{R}(t, m_i, m_j) = \sum_{n=1,2} \mathcal{R}_n(t, m_i, m_j), \tag{9}$$

and the total merger rate is

$$R(t) = \int \mathcal{R}(t, m_i, m_j) {\rm d}m_i {\rm d}m_j = \sum_{n=1,2} R_n(t), \tag{10}$$

where

$$R_n(t) = \int \mathcal{R}_n(t, m_i, m_j) {\rm d}m_i {\rm d}m_j. \tag{11}$$

All the above-mentioned merger rate (density) is measured at the source frame. We should emphasize that although $R_2(t)$ should be smaller than $R_1(t)$ as expected, $\mathcal{R}_2(t, m_i, m_j)$ is not necessarily be smaller than $\mathcal{R}_1(t, m_i, m_j)$ (Liu et al. 2019).

3. HIERARCHICAL BAYESIAN INFERENCE

We adopt a hierarchical Bayesian approach to infer the population parameters by marginalizing the uncertainty in estimating individual event parameters. This section describes the hierarchical Bayesian inference used in the parameter estimations. The merger rate density (9) is measured in the source frame, and we need to convert it into the detector frame as

$$\mathcal{R}_{\rm pop}(\theta|\Lambda) = \frac{1}{1+z} \frac{dV_{\rm c}}{dz} \mathcal{R}(\theta|\Lambda), \tag{12}$$

where z is the cosmological redshift, $\theta \equiv \{z, m_1, m_2\}$, Λ is a collection of $f_{\rm pbh}$ and the parameters from mass function $P(m)$, and $dV_{\rm c}/dz$ is the differential comoving volume. The factor $1/(1+z)$ converts time increments from the source to the detector frame. We take the cosmological parameters from Planck 2018 (Aghanim et al. 2020).

Given the data, $\mathbf{d} = \{d_1, d_2, \cdots, d_{N_{\rm obs}}\}$, of $N_{\rm obs}$ BBH merger events, we model the total number of events as an inhomogeneous Poisson process, yielding the likelihood (Loredo 2004; Thrane & Talbot 2018; Mandel et al. 2018)

$$\mathcal{L}(\mathbf{d}|\Lambda) \propto N_{\rm exp}^{N_{\rm obs}} e^{-N_{\rm exp}} \prod_{i=1}^{N_{\rm obs}} \frac{\int \mathcal{L}(d_i|\theta)\, \mathcal{R}_{\rm pop}(\theta|\Lambda) d\theta}{\xi(\Lambda)}, \tag{13}$$

where $N_{\rm exp} \equiv N_{\rm exp}(\Lambda)$ is the expected number of detections over the timespan of observation. Here $\mathcal{L}(d_i|\theta)$ is the individual event likelihood for the ith GW event that can be derived from the individual event's posterior by reweighing with the prior on θ. Here, $\xi(\Lambda)$ quantifies selection biases for a population with parameters Λ and is defined by

$$\xi(\Lambda) = \int P_{\rm det}(\theta)\, \mathcal{R}_{\rm pop}(\theta|\Lambda)\, {\rm d}\theta, \tag{14}$$

where $P_{\rm det}(\theta)$ is the detection probability that depends on the source parameters θ. In practice, we use the simulated injections (Abbott et al. 2021c) to estimate $\xi(\Lambda)$, and Eq. (14) can be approximated by a Monte Carlo integral over found injections (Abbott et al. 2021d)

$$\xi(\Lambda) \approx \frac{1}{N_{\rm inj}} \sum_{j=1}^{N_{\rm found}} \frac{\mathcal{R}_{\rm pop}(\theta_j|\Lambda)}{p_{\rm draw}(\theta_j)}, \tag{15}$$

where $N_{\rm inj}$ is the total number of injections, $N_{\rm found}$ is the number of successfully detected injections, and $p_{\rm draw}$ is the probability density function from which the injections are drawn. Using the posterior samples from each event, we estimate the hyper-likelihood (13) as

$$\mathcal{L}(\mathbf{d}|\Lambda) \propto N_{\rm exp}^{N_{\rm obs}} e^{-N_{\rm exp}} \prod_{i=1}^{N_{\rm obs}} \frac{1}{\xi(\Lambda)} \left\langle \frac{\mathcal{R}_{\rm pop}(\theta|\Lambda)}{d_L^2(z)} \right\rangle, \tag{16}$$

Parameter	Description	Prior
$f_{\rm pbh}$	Abundance of PBH in dark matter	log-$\mathcal{U}(-4, 0)$
	Lognormal PBH mass function	
$M_{\rm c}$	Central mass in $M_\odot$.	$\mathcal{U}(5, 50)$
σ	Mass width.	$\mathcal{U}(0.1, 2)$
	Power-law PBH mass function	
$M_{\rm min}$	Lower mass cut-off in $M_\odot$.	$\mathcal{U}(3, 10)$
α	Power-law index.	$\mathcal{U}(1.05, 4)$
	Broken Power-law PBH mass function	
M_*	Peak mass in $M_\odot$.	$\mathcal{U}(3, 15)$
α_1	First power-law index.	$\mathcal{U}(0, 15)$
α_2	Second power-law index.	$\mathcal{U}(1, 3)$
	Critical collapse (CC) PBH mass function	
$M_{\rm f}$	Horizon mass scale in $M_\odot$.	$\mathcal{U}(1, 50)$
α	Universal exponent.	$\mathcal{U}(0, 5)$

Table 1. Parameters and their prior distributions used in the Bayesian parameter estimations. Here, $\mathcal{U}$ and log-$\mathcal{U}$ denote uniform and log-uniform distributions, respectively.

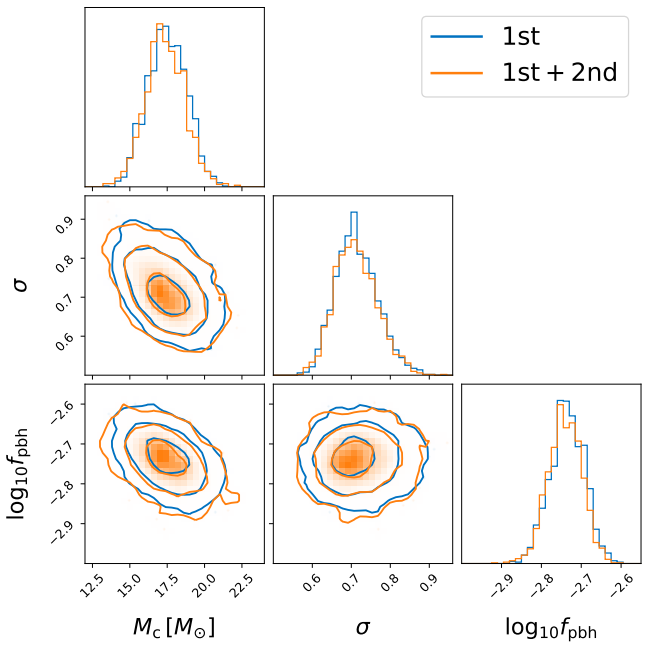

Figure 1. The marginalized one- and two-dimensional posterior distributions for hyper-parameters $\{M_c, \sigma, f_{\rm pbh}\}$ in the log-normal mass function inferred from GWTC-3. The blue color denotes the results from the first merger only, while the orange denotes the results from both the first and second mergers. The contours represent the 1σ, 2σ and 3σ credible regions, respectively.

where $\langle \cdots \rangle$ denotes the weighted average over posterior samples of θ. The denominator $d_L^2(z)$ is the standard priors used in the LVK analysis of individual events where d_L is the luminosity distance.

In this work, we incorporate the PBH population distribution (9) into the `ICAROGW` (Mastrogiovanni et al. 2021) package to estimate the likelihood function (16), and use `dynesty` (Speagle 2020) sampler called from `Bilby` (Ashton et al. 2019; Romero-Shaw et al. 2020) to sample over the parameter space. We use the GW events from GWTC-3 by discarding events with false alarm rate larger than 1 $\rm yr^{-1}$ and events with the secondary component mass smaller than $3M_\odot$ to avoid contamination from putative events involving neutron stars following De Luca et al. (2021). A total of 69 GW events from GWTC-3 meet this criteria and the posterior samples of these BBHs are publicly available from Abbott et al. (2021e).

4. RESULTS

Based on the hierarchical statistical framework, we do the parameter estimations for four different PBH mass functions commonly used in the literature. These mass functions are the log-normal, power-law, broken power-law, and critical collapse (CC) distributions, respectively. We summarize the parameters and their prior distributions in Table 1. Below we show the results for each of the PBH mass functions.

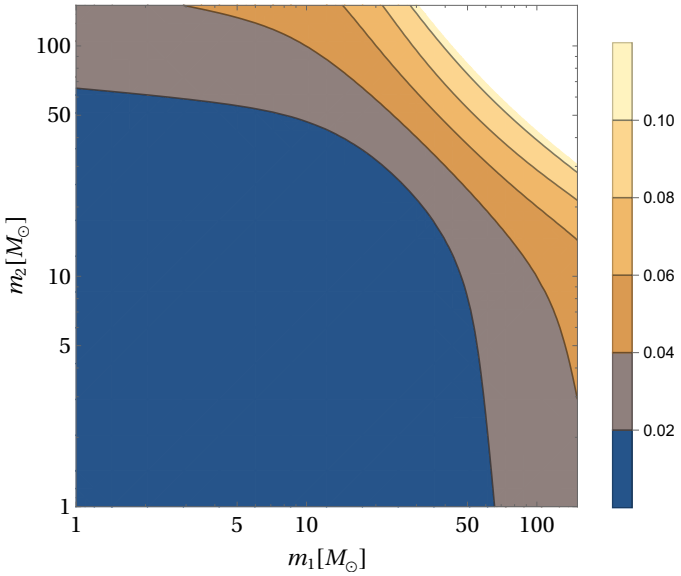

Figure 2. The ratio of merger rate density from second merger to that from first merger, $\mathcal{R}_2(t_0, m_1, m_2)/\mathcal{R}_1(t_0, m_1, m_2)$, as a function of component masses for the log-normal mass function. We have fixed the hyper-parameters $\{M_c, \sigma, f_{\rm pbh}\}$ to their best-fit values.

4.1. *Log-normal mass function*

We first consider a PBH mass function with the log-normal form (Dolgov & Silk 1993) of

$$P(m) = \frac{1}{\sqrt{2\pi}\sigma m} \exp\left(-\frac{\ln^2(m/M_c)}{2\sigma^2}\right), \tag{17}$$

where M_c represents the central mass of $mP(m)$, and σ characterizes the width of the mass spectrum. The log-normal mass function can approximate a huge class of extended mass distributions if PBHs are formed from a smooth, symmetric peak in the inflationary power spectrum when the slow-roll approximation holds (Green 2016; Carr et al. 2017; Kannike et al. 2017). The hyper-parameters are $\Lambda = \{M_c, \sigma, f_{\rm pbh}\}$ in this case. We can then derive the averaged PBH mass and averaged number density from Eq. (3) and Eq. (4) as

$$m_{\rm pbh} = M_c \exp\left(-\frac{\sigma^2}{2}\right), \tag{18}$$

$$F(m) = \frac{M_c}{\sqrt{2\pi}\sigma m^2} \exp\left(-\frac{\sigma^2}{2} - \frac{\ln^2(m/M_c)}{2\sigma^2}\right). \tag{19}$$

Using 69 BBHs from GWTC-3 and performing the hierarchical Bayesian inference, we obtain M_c =

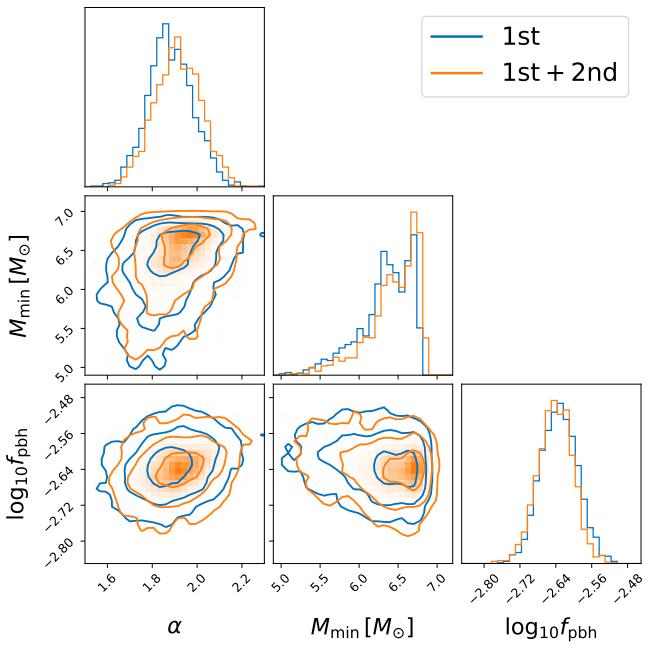

Figure 3. The marginalized one- and two-dimensional posterior distributions for hyper-parameters $\{M_{\rm min}, \alpha, f_{\rm pbh}\}$ in the power-law mass function inferred from GWTC-3. The blue color denotes the results from the first merger only, while the orange denotes the results from both the first and second mergers. The contours represent the 1σ, 2σ and 3σ credible regions, respectively.

$17.3^{+2.2}_{-2.0} M_\odot$, $\sigma = 0.71^{+0.10}_{-0.08}$, and $f_{\rm pbh} = 1.8^{+0.3}_{-0.3} \times 10^{-3}$. In this work, we present results with median value and 90% equal-tailed credible intervals. The posteriors for the hyper-parameters $\Lambda = \{M_c, \sigma, f_{\rm pbh}\}$ are shown in Fig. 1. Note that we get a larger value of M_c than that inferred from GWTC-1 in Wu (2020) because GWTC-3 contains heavier BHs than those from GWTC-1. From Eq. (10), we also infer the local merger rate as $R(t_0) = 41^{+16}_{-12}{\rm Gpc}^{-3}\,{\rm yr}^{-1}$. The results of local merger rate and abundance of PBHs are consistent with the previous estimations (Chen & Huang 2018; Chen et al. 2019; Chen & Huang 2019; Wu 2020; Chen et al. 2022b,a), confirming that CDM cannot be dominated by the stellar-mass PBHs.

In Fig. 2, we show the ratio of merger rate density from second merger to the one from first merger, namely $\mathcal{R}_2(t_0, m_1, m_2)/\mathcal{R}_1(t_0, m_1, m_2)$, by fixing the hyper-parameters $\{M_c, \sigma, f_{\rm pbh}\}$ to their best-fit values. It can be seen that the second merger provides more contribution to the total merger rate density as component mass increases. Even though $\mathcal{R}_2(t_0, m_1, m_2)/\mathcal{R}_1(t_0, m_1, m_2)$ can reach as high as $\gtrsim 10\%$, the ratio of merger rate from second merger to that from first merger is $R_2(t_0)/R_1(t_0) = 1.0^{+0.2}_{-0.1}\%$ and is negligible. This is because the major contribution to the merger rate is from the masses less than $50 M_\odot$, and the correction is negligible in this mass range. Therefore the effect of merger history can be safely ignored when estimating the merger rate of PBH binaries.

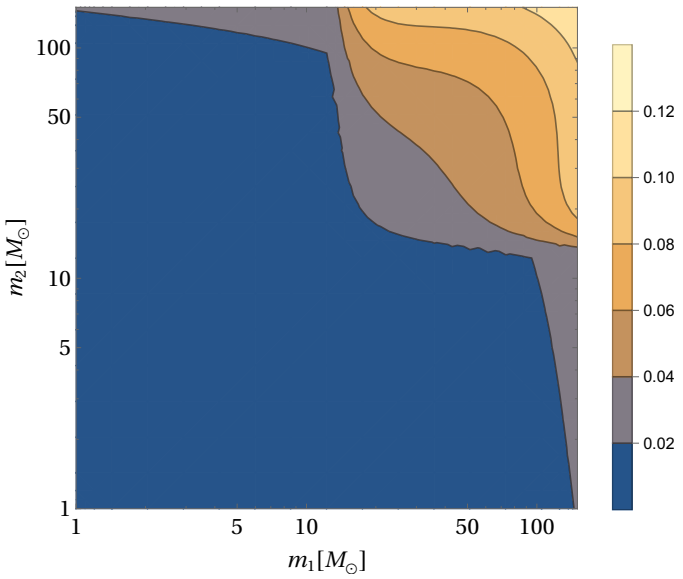

Figure 4. The ratio of merger rate density from second merger to that from first merger, $\mathcal{R}_2(t_0, m_1, m_2)/\mathcal{R}_1(t_0, m_1, m_2)$, as a function of component masses for the power-law mass function. We have fixed the hyper-parameters $\{M_{\rm min}, \alpha, f_{\rm pbh}\}$ to their best-fit values.

4.2. *Power-law mass function*

We next consider a PBH mass function with the power-law form (Carr 1975) of

$$P(m) = \frac{\alpha - 1}{M_{\rm min}} \left(\frac{m}{M_{\rm min}}\right)^{-\alpha}, \tag{20}$$

where $M_{\rm min}$ is the lower-mass cut-off such that $m > M_{\rm min}$, and $\alpha > 1$ is the power-law index. The power-law mass function can typically result from a broad or flat power spectrum of the curvature perturbations (De Luca et al. 2020) during radiation dominated era (Carr et al. 2016a, 2017). The hyper-parameters are $\Lambda = \{M_{\rm min}, \alpha, f_{\rm pbh}\}$ in this case. We can then derive the averaged PBH mass and averaged number density from Eq. (3) and Eq. (4) as

$$m_{\rm pbh} = M_{\rm min} \frac{\alpha}{\alpha - 1}, \tag{21}$$

$$F(m) = \frac{\alpha}{m} \left(\frac{m}{M_{\rm min}}\right)^{-\alpha}. \tag{22}$$

Using 69 BBHs from GWTC-3 and performing the hierarchical Bayesian inference, we obtain $M_{\rm min}$ =

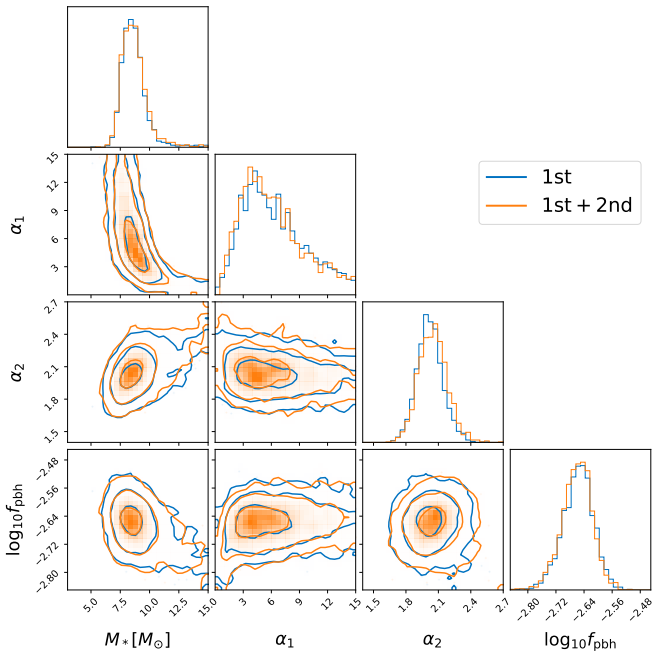

Figure 5. The marginalized one- and two-dimensional posterior distributions for hyper-parameters $\{m_*, \alpha_1, \alpha_2, f_{\rm pbh}\}$ in the broken power-law mass function inferred from GWTC-3. The blue color denotes the results from the first merger only, while the orange denotes the results from both the first and second mergers. The contours represent the 1σ, 2σ and 3σ credible regions, respectively.

$6.5^{+0.3}_{-0.8} M_\odot$, $\alpha = 1.9^{+0.2}_{-0.2}$, and $f_{\rm pbh} = 2.3^{+0.3}_{-0.3} \times 10^{-3}$. The posteriors for the hyper-parameters $\Lambda = \{M_{\rm min}, \alpha, f_{\rm pbh}\}$ are shown in Fig. 3. Note that we get a smaller value of α than that inferred from GWTC-1 in Wu (2020) because GWTC-3 contains heavier BHs than those from GWTC-1. From Eq. (10), we also infer the local merger rate as $R(t_0) = 48^{+15}_{-12} {\rm Gpc}^{-3}\,{\rm yr}^{-1}$. The results of local merger rate and abundance of PBHs are consistent with the previous estimations (Chen & Huang 2018; Chen et al. 2019; Chen & Huang 2019; Wu 2020; Chen et al. 2022b,a), confirming that CDM cannot be dominated by the stellar-mass PBHs.

In Fig. 4, we show the ratio of merger rate density from second merger to the one from first merger, namely $\mathcal{R}_2(t_0, m_1, m_2)/\mathcal{R}_1(t_0, m_1, m_2)$, by fixing the hyper-parameters $\{M_{\rm min}, \alpha, f_{\rm pbh}\}$ to their best-fit values. It can be seen that the second merger provides more contribution to the total merger rate density as component mass increases. Even though $\mathcal{R}_2(t_0, m_1, m_2)/\mathcal{R}_1(t_0, m_1, m_2)$ can reach as high as $\gtrsim 10\%$, the ratio of merger rate from second merger to that from first merger is $R_2(t_0)/R_1(t_0) = 0.9^{+0.1}_{-0.1}\%$ and is negligible. This is because the major contribution to the merger rate is from the masses less than $50 M_\odot$, and

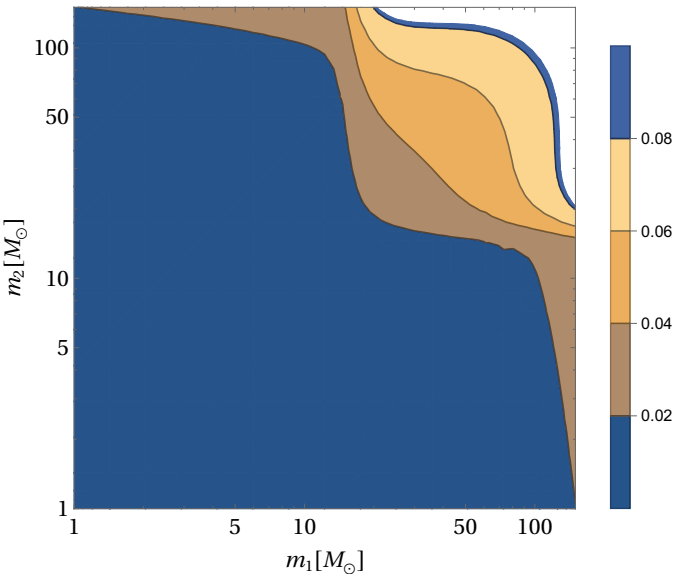

Figure 6. The ratio of merger rate density from second merger to that from first merger, $\mathcal{R}_2(t_0, m_1, m_2)/\mathcal{R}_1(t_0, m_1, m_2)$, as a function of component masses for the broken power-law mass function. We have fixed the hyper-parameters $\{m_*, \alpha_1, \alpha_2, f_{\rm pbh}\}$ to their best-fit values.

the correction is negligible in this mass range. Therefore the effect of merger history can be safely ignored when estimating the merger rate of PBH binaries.

4.3. *Broken power-law mass function*

We then consider a PBH mass function with the broken power-law form (Deng 2021) of

$$P(m) = \left(\frac{m_*}{\alpha_1 + 1} - \frac{m_*}{\alpha_2 - 1}\right)^{-1} \begin{cases} (\frac{m}{m_*})^{\alpha_1}, & m < m_* \\ (\frac{m}{m_*})^{-\alpha_2}, & m > m_* \end{cases}, \tag{23}$$

where m_* is the peak mass of $mP(m)$. Here $\alpha_1 > 0$ and $\alpha_2 > 1$ are two power-law indices. The broken power-law mass function is a generalization of the power-law form. It can be achieved if PBHs are formed by vacuum bubbles that nucleate during inflation via quantum tunneling (Deng 2021). The hyper-parameters are $\Lambda = \{m_*, \alpha_1, \alpha_2, f_{\rm pbh}\}$ in this case. We can then derive the averaged PBH mass and averaged number density from Eq. (3) and Eq. (4) as

$$m_{\rm pbh} = \frac{\alpha_1 \alpha_2}{(\alpha_1 + 1)(\alpha_2 - 1)} m_*, \tag{24}$$

$$F(m) = \frac{\alpha_1 \alpha_2}{\alpha_1 + \alpha_2} \begin{cases} (\frac{m}{m_*})^{\alpha_1}, & m < m_* \\ (\frac{m}{m_*})^{-\alpha_2}, & m > m_* \end{cases}. \tag{25}$$

Using 69 BBHs from GWTC-3 and performing the hierarchical Bayesian inference, we obtain $m_* =$

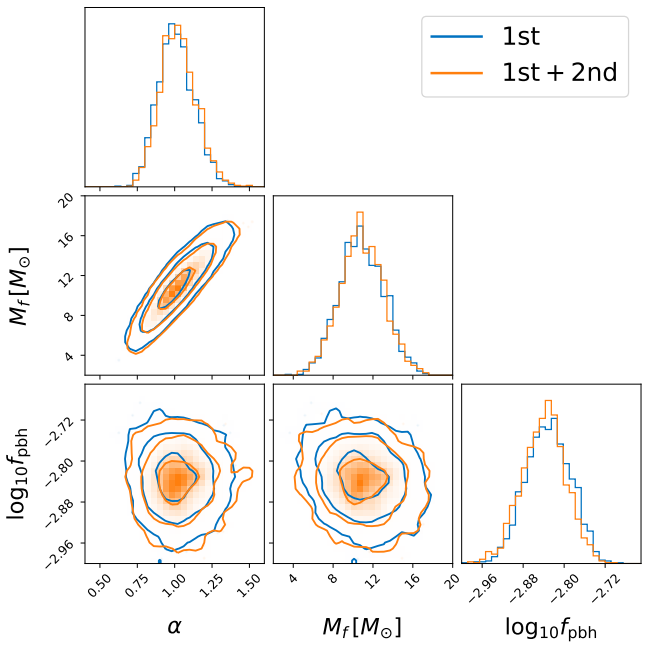

Figure 7. The marginalized one- and two-dimensional posterior distributions for hyper-parameters $\{M_{\rm f}, \alpha, f_{\rm pbh}\}$ in the critical collapse mass function inferred from GWTC-3. The blue color denotes the results from the first merger only, while the orange denotes the results from both the first and second mergers. The contours represent the 1σ, 2σ and 3σ credible regions, respectively.

$8.6^{+2.1}_{-1.3} M_\odot$, $\alpha_1 = 5.6^{+7.1}_{-3.8}$, $\alpha_2 = 2.0^{+0.2}_{-0.2}$, and $f_{\rm pbh} = 2.2^{+0.3}_{-0.4} \times 10^{-3}$. The posteriors for the hyper-parameters $\Lambda = \{m_*, \alpha_1, \alpha_2, f_{\rm pbh}\}$ are shown in Fig. 5. From Eq. (10), we also infer the local merger rate as $R(t_0) = 46^{+15}_{-11} {\rm Gpc}^{-3}\,{\rm yr}^{-1}$. The results of local merger rate and abundance of PBHs are consistent with the previous estimations (Chen & Huang 2018; Chen et al. 2019; Chen & Huang 2019; Wu 2020; Chen et al. 2022b,a), confirming that CDM cannot be dominated by the stellar-mass PBHs. Note that Deng (2021) obtains quite different results for the broken power-law mass function using GWTC-2 data without accounting for the uncertainties in the measurement of $\vec{\theta}$. Deng (2021) also deals with the selection effect of the GW detectors improperly. We emphasize that our results are more robust because we have a comprehensive treatment of the selection effect and measurement uncertainties. Nevertheless, as expected, our results of the broken power-law mass function are fully consistent with the results of the power-law case.

In Fig. 6, we show the ratio of merger rate density from second merger to the one from first merger, namely $\mathcal{R}_2(t_0, m_1, m_2)/\mathcal{R}_1(t_0, m_1, m_2)$, by fixing the hyper-parameters $\{m_*, \alpha_1, \alpha_2, f_{\rm pbh}\}$ to their best-fit values. It can be seen that the second merger provides more contribution to the total merger rate density as component mass increases. Even though $\mathcal{R}_2(t_0, m_1, m_2)/\mathcal{R}_1(t_0, m_1, m_2)$ can reach as high as $\gtrsim 10\%$, the ratio of merger rate from second merger to that from first merger is $R_2(t_0)/R_1(t_0) = 0.9^{+0.3}_{-0.1}\%$ and is negligible. This is because the major contribution to the merger rate is from the masses less than $50 M_\odot$, and the correction is negligible in this mass range. Therefore the effect of merger history can be safely ignored when estimating the merger rate of PBH binaries.

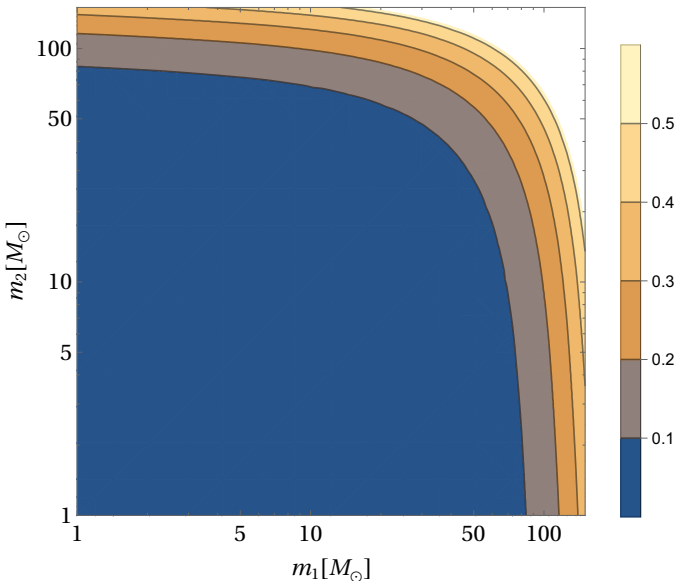

Figure 8. The ratio of merger rate density from second merger to that from first merger, $\mathcal{R}_2(t_0, m_1, m_2)/\mathcal{R}_1(t_0, m_1, m_2)$, as a function of component masses for the critical collapse mass function. We have fixed the hyper-parameters $\{M_{\rm f}, \alpha, f_{\rm pbh}\}$ to their best-fit values.

4.4. *Critical collapse mass function*

We last consider a PBH mass function with the critical collapse form (Niemeyer & Jedamzik 1998; Yokoyama 1998; Carr et al. 2016b; Gow et al. 2022) of

$$P(m) = \frac{\alpha^2\, m^\alpha}{{M_{\rm f}}^{1+\alpha}\,\Gamma(1/\alpha)} \exp\left(-(m/M_{\rm f})^\alpha\right), \qquad (26)$$

where α is a universal exponent relating to the critical collapse of radiation, and $M_{\rm f}$ is the mass scale at the order of horizon mass at the collapse epoch (Carr et al. 2016b). There is no lower mass cut-off for this mass spectrum, but it is exponentially suppressed above the mass scale of $M_{\rm f}$. The critical collapse mass function is closely associated with a δ-function power spectrum of the density fluctuations (Niemeyer & Jedamzik 1998; Yokoyama 1998; Carr et al. 2016b; Gow et al. 2022). The hyper-parameters are $\Lambda = \{M_{\rm f}, \alpha, f_{\rm pbh}\}$ in this case. We

can then derive the averaged PBH mass and averaged number density from Eq. (3) and Eq. (4) as

$$m_{\rm pbh} = \frac{M_{\rm f}\Gamma(1/\alpha)}{\alpha}, \tag{27}$$

$$F(m) = \alpha {M_{\rm f}}^{-\alpha} m^{\alpha-1} \exp\left(-(m/M_{\rm f})^{\alpha}\right). \tag{28}$$

Using 69 BBHs from GWTC-3 and performing the hierarchical Bayesian inference, we obtain $M_{\rm f} = 10.8^{+3.7}_{-3.6} M_\odot$, $\alpha = 1.0^{+0.2}_{-0.2}$, and $f_{\rm pbh} = 1.5^{+0.2}_{-0.2} \times 10^{-3}$. The posteriors for the hyper-parameters $\Lambda = \{M_{\rm f}, \alpha, f_{\rm pbh}\}$ are shown in Fig. 7. From Eq. (10), we also infer the local merger rate as $R(t_0) = 49^{+26}_{-16}{\rm Gpc}^{-3}\,{\rm yr}^{-1}$. The results of local merger rate and abundance of PBHs are consistent with the previous estimations (Chen & Huang 2018; Chen et al. 2019; Chen & Huang 2019; Wu 2020; Chen et al. 2022b,a), confirming that CDM cannot be dominated by the stellar-mass PBHs.

In Fig. 8, we show the ratio of merger rate density from second merger to the one from first merger, namely $\mathcal{R}_2(t_0, m_1, m_2)/\mathcal{R}_1(t_0, m_1, m_2)$, by fixing the hyper-parameters $\{M_{\rm f}, \alpha, f_{\rm pbh}\}$ to their best-fit values. It can be seen that the second merger provides more contribution to the total merger rate density as component mass increases. Even though $\mathcal{R}_2(t_0, m_1, m_2)/\mathcal{R}_1(t_0, m_1, m_2)$ can reach as high as $\gtrsim$ 10%, the ratio of merger rate from second merger to that from first merger is $R_2(t_0)/R_1(t_0) = 2.2^{+1.3}_{-0.1}\%$ and is negligible. This is because the major contribution to the merger rate is from the masses less than $50M_\odot$, and the correction is negligible in this mass range. Therefore the effect of merger history can be safely ignored when estimating the merger rate of PBH binaries.

5. CONCLUSION

In this work, we use 69 BBHs from GWTC-3 to constrain the merger history of PBH binaries by assuming the observed BBHs from LVK are attributed to PBHs. We perform comprehensive Bayesian analyses by considering four commonly used PBH mass functions in literature, namely the log-normal, power-law, broken power-law, and critical collapse mass functions.

We summarize the key results in Table 2. It can be seen that the contribution of the merger rate from the second merger to the total merger rate is less than 5%. Therefore, the merger history of PBH binaries has a subdominant effect, and this effect can be neglected when evaluating the merger rate of PBH binaries. It can also be seen that the Bayes factors for the model with a second merger versus the model with only the first merger, $\rm BF^{2nd}_{1st}$, are all smaller than 3, indicating the evidence for the second merger is "not worth more than a bare mention" (Kass & Raftery 1995). In this sense, the Bayes factors also imply that the effect of merger history can be ignored.

	LN	PL	BPL	CC
$\rm BF^{2nd}_{1st}$	0.9	0.4	0.69	1.2
$\rm BF_{PL}$	166	1	2	139
$10^3 f_{\rm pbh}$	$1.8^{+0.3}_{-0.3}$	$2.3^{+0.3}_{-0.3}$	$2.2^{+0.3}_{-0.4}$	$1.5^{+0.2}_{-0.2}$
$10^2 R_2/R_1$	$1.0^{+0.2}_{-0.1}$	$0.9^{+0.1}_{-0.1}$	$0.9^{+0.3}_{-0.1}$	$2.2^{+1.3}_{-0.5}$

Table 2. Summary of the key results for the log-normal (LN), power-law (PL), broken power-law (BPL), and critical collapse (CC) mass functions. The first row, $\rm BF^{2nd}_{1st}$, shows the Bayes factors for the model with 2nd merger versus the model with only 1st merger; the second row, $\rm BF_{PL}$, shows the Bayes factors for the model with different PBH mass function versus the model with the power-law PBH mass function by accounting for the second merger effect; the third row, $f_{\rm pbh}$, shows the abundance of PBH in dark matter inferred from different models by accounting for the second merger effect; the last row, R_2/R_1, shows the merger rate ratio between the second merger and the first merger.

Furthermore, for all four mass functions, we infer the abundance of PBH in cold dark matter, $f_{\rm pbh}$, to be at the order of $\mathcal{O}(10^{-3})$. The results of local merger rate and abundance of PBHs are consistent with the previous estimations (Chen & Huang 2018; Chen et al. 2019; Chen & Huang 2019; Wu 2020; Chen et al. 2022b,a), confirming that CDM cannot be dominated by the stellar-mass PBHs.

We also compute the Bayes factors between the models with different PBH mass functions. The Bayes factors $\rm BF_{PL}$ are estimated by taking the model with the power-law mass function as the fiducial model. We find that $\rm BF^{LG}_{PL}$ has the largest value, indicating that the log-normal mass function can best fit GWTC-3 among the four mass functions considered in this work. Our findings contradict the results from Deng (2021) claiming that the broken power-law mass function can fit better than the log-normal form. There are some drawbacks from analyses in Deng (2021). Firstly, Deng (2021) neglects the uncertainties in measuring each event's masses and completely ignores the redshift evolution of the merger rate. Secondly, Deng (2021) deals with the selection effect of GW detectors improperly. In this sense, we disagree with Deng (2021) and conclude that the most frequently used log-normal mass function can fit GWTC-3 best among the four mass functions.

We would also like to thank Xingjiang Zhu, Xiao-Jin Liu, Shen-Shi Du, and Zhu Yi for useful discussions. Z.-C.C. is supported by the China Postdoctoral Science Foundation Fellowship No. 2022M710429. This research has made use of data, software and/or web tools obtained from the Gravitational Wave Open Science Center (https://www.gw-openscience.org/), a service of LIGO Laboratory, the LIGO Scientific Collaboration, the Virgo Collaboration, and the KAGRA Collaboration. LIGO Laboratory and Advanced LIGO are funded by the United States National Science Foundation (NSF) as well as the Science and Technology Facilities Council (STFC) of the United Kingdom, the Max-Planck-Society (MPS), and the State of Niedersachsen/Germany for support of the construction of Advanced LIGO and construction and operation of the GEO600 detector. Additional support for Advanced LIGO was provided by the Australian Research Council. Virgo is funded, through the European Gravitational Observatory (EGO), by the French Centre National de Recherche Scientifique (CNRS), the Italian Istituto Nazionale di Fisica Nucleare (INFN) and the Dutch Nikhef, with contributions by institutions from Belgium, Germany, Greece, Hungary, Ireland, Japan, Monaco, Poland, Portugal, Spain. The construction and operation of KAGRA are funded by Ministry of Education, Culture, Sports, Science and Technology (MEXT), and Japan Society for the Promotion of Science (JSPS), National Research Foundation (NRF) and Ministry of Science and ICT (MSIT) in Korea, Academia Sinica (AS) and the Ministry of Science and Technology (MoST) in Taiwan.

REFERENCES

Abbott, B. P., et al. 2019, Phys. Rev. X, 9, 031040, doi: 10.1103/PhysRevX.9.031040

Abbott, R., et al. 2020, Phys. Rev. Lett., 125, 101102, doi: 10.1103/PhysRevLett.125.101102

—. 2021a, Phys. Rev. X, 11, 021053, doi: 10.1103/PhysRevX.11.021053

—. 2021b. https://arxiv.org/abs/2111.03606

—. 2021c, doi: https://doi.org/10.5281/zenodo.5546676

—. 2021d. https://arxiv.org/abs/2111.03634

—. 2021e, The population of merging compact binaries inferred using gravitational waves through GWTC-3 - Data release, v1, Zenodo, doi: 10.5281/zenodo.5655785

Aghanim, N., et al. 2020, Astron. Astrophys., 641, A6, doi: 10.1051/0004-6361/201833910

Ali-Haïmoud, Y., Kovetz, E. D., & Kamionkowski, M. 2017, Phys. Rev., D96, 123523, doi: 10.1103/PhysRevD.96.123523

Anagnostou, O., Trenti, M., & Melatos, A. 2020. https://arxiv.org/abs/2010.06161

Ashton, G., et al. 2019, Astrophys. J. Suppl., 241, 27, doi: 10.3847/1538-4365/ab06fc

Bartolo, N., De Luca, V., Franciolini, G., et al. 2019a, Phys. Rev. Lett., 122, 211301, doi: 10.1103/PhysRevLett.122.211301

—. 2019b, Phys. Rev., D99, 103521, doi: 10.1103/PhysRevD.99.103521

Bird, S., Cholis, I., Muñoz, J. B., et al. 2016, Phys. Rev. Lett., 116, 201301, doi: 10.1103/PhysRevLett.116.201301

Cai, R.-G., Guo, Z.-K., Liu, J., Liu, L., & Yang, X.-Y. 2019a. https://arxiv.org/abs/1912.10437

Cai, R.-g., Pi, S., & Sasaki, M. 2019b, Phys. Rev. Lett., 122, 201101, doi: 10.1103/PhysRevLett.122.201101

Cai, R.-G., Pi, S., Wang, S.-J., & Yang, X.-Y. 2019c, doi: 10.1088/1475-7516/2019/10/059

Carr, B., Kuhnel, F., & Sandstad, M. 2016a, Phys. Rev., D94, 083504, doi: 10.1103/PhysRevD.94.083504

Carr, B., Raidal, M., Tenkanen, T., Vaskonen, V., & Veermäe, H. 2017, Phys. Rev., D96, 023514, doi: 10.1103/PhysRevD.96.023514

Carr, B. J. 1975, Astrophys. J., 201, 1, doi: 10.1086/153853

Carr, B. J., & Hawking, S. W. 1974, Mon. Not. Roy. Astron. Soc., 168, 399

Carr, B. J., Kohri, K., Sendouda, Y., & Yokoyama, J. 2016b, Phys. Rev. D, 94, 044029, doi: 10.1103/PhysRevD.94.044029

Chen, Z.-C., Du, S.-S., Huang, Q.-G., & You, Z.-Q. 2022a. https://arxiv.org/abs/2205.11278

Chen, Z.-C., Huang, F., & Huang, Q.-G. 2019, Astrophys. J., 871, 97, doi: 10.3847/1538-4357/aaf581

Chen, Z.-C., & Huang, Q.-G. 2018, Astrophys. J., 864, 61, doi: 10.3847/1538-4357/aad6e2

—. 2019. https://arxiv.org/abs/1904.02396

Chen, Z.-C., Yuan, C., & Huang, Q.-G. 2020, Phys. Rev. Lett., 124, 251101, doi: 10.1103/PhysRevLett.124.251101

—. 2022b, Phys. Lett. B, 829, 137040, doi: 10.1016/j.physletb.2022.137040

De Luca, V., Franciolini, G., Kehagias, A., & Riotto, A. 2019. https://arxiv.org/abs/1911.09689

De Luca, V., Franciolini, G., Pani, P., & Riotto, A. 2021, JCAP, 05, 003, doi: 10.1088/1475-7516/2021/05/003

De Luca, V., Franciolini, G., & Riotto, A. 2020, Phys. Lett. B, 807, 135550, doi: 10.1016/j.physletb.2020.135550

Deng, H. 2021, JCAP, 04, 058, doi: 10.1088/1475-7516/2021/04/058

Dolgov, A., & Silk, J. 1993, Phys. Rev., D47, 4244, doi: 10.1103/PhysRevD.47.4244

Farmer, R., Renzo, M., de Mink, S., Fishbach, M., & Justham, S. 2020, Astrophys. J. Lett., 902, L36, doi: 10.3847/2041-8213/abbadd

Farmer, R., Renzo, M., de Mink, S. E., Marchant, P., & Justham, S. 2019, The Astrophysical Journal, 887, 53, doi: 10.3847/1538-4357/ab518b

Gow, A. D., Byrnes, C. T., & Hall, A. 2022, Phys. Rev. D, 105, 023503, doi: 10.1103/PhysRevD.105.023503

Green, A. M. 2016, Phys. Rev., D94, 063530, doi: 10.1103/PhysRevD.94.063530

Hawking, S. 1971, Mon. Not. Roy. Astron. Soc., 152, 75

Kannike, K., Marzola, L., Raidal, M., & Veermäe, H. 2017, JCAP, 1709, 020, doi: 10.1088/1475-7516/2017/09/020

Kass, R. E., & Raftery, A. E. 1995, Journal of the American Statistical Association, 90, 773, doi: 10.1080/01621459.1995.10476572

Liu, L., Guo, Z.-K., & Cai, R.-G. 2019, Eur. Phys. J., C79, 717, doi: 10.1140/epjc/s10052-019-7227-0

Loredo, T. J. 2004, AIP Conf. Proc., 735, 195, doi: 10.1063/1.1835214

Mandel, I., Farr, W. M., & Gair, J. R. 2018. https://arxiv.org/abs/1809.02063

Marchant, P., & Moriya, T. 2020, Astron. Astrophys., 640, L18, doi: 10.1051/0004-6361/202038902

Marchant, P., Renzo, M., Farmer, R., et al. 2019, The Astrophysical Journal, 882, 36, doi: 10.3847/1538-4357/ab3426

Mastrogiovanni, S., Leyde, K., Karathanasis, C., et al. 2021, Phys. Rev. D, 104, 062009, doi: 10.1103/PhysRevD.104.062009

Nakamura, T., Sasaki, M., Tanaka, T., & Thorne, K. S. 1997, Astrophys. J., 487, L139, doi: 10.1086/310886

Niemeyer, J. C., & Jedamzik, K. 1998, Phys. Rev. Lett., 80, 5481, doi: 10.1103/PhysRevLett.80.5481

Romero-Shaw, I. M., et al. 2020, Mon. Not. Roy. Astron. Soc., 499, 3295, doi: 10.1093/mnras/staa2850

Sasaki, M., Suyama, T., Tanaka, T., & Yokoyama, S. 2016, Phys. Rev. Lett., 117, 061101, doi: 10.1103/PhysRevLett.117.061101

Speagle, J. S. 2020, Mon. Not. Roy. Astron. Soc., 493, 3132, doi: 10.1093/mnras/staa278

Thrane, E., & Talbot, C. 2018. https://arxiv.org/abs/1809.02293

Wu, Y. 2020, Phys. Rev. D, 101, 083008, doi: 10.1103/PhysRevD.101.083008

Yokoyama, J. 1998, Phys. Rev. D, 58, 107502, doi: 10.1103/PhysRevD.58.107502

Yuan, C., Chen, Z.-C., & Huang, Q.-G. 2019, Phys. Rev., D100, 081301, doi: 10.1103/PhysRevD.100.081301

—. 2020a, Phys. Rev. D, 101, 043019, doi: 10.1103/PhysRevD.101.043019

—. 2020b, Phys. Rev. D, 101, 063018, doi: 10.1103/PhysRevD.101.063018